

Suppression of thermoacoustic instability in a swirl-stabilized combustor by inducing blockage in the inlet flow stream

Nitin B. George,^{*} Vishnu R. Unni,[†] Manikandan Raghunathan [‡]and R. I. Sujith[§]

Indian Institute of Technology Madras, Chennai-600036, India

Swirl flows are often used for flame stabilization in gas turbine combustors. However, when these combustors are operated at lean fuel/air ratios, they are prone to thermoacoustic instability. In this study, we experimentally investigate the effect of distribution of the blockage in the inlet flow on the transition of the combustion dynamics from combustion noise to thermoacoustic instability. We acquire unsteady pressure fluctuations and heat release rate fields (CH^* chemiluminescence) by capturing the flame images to investigate this transition in the thermoacoustic system. We utilize a turbulence generator with two different configurations to modify the inlet flow dynamics to achieve passive control of thermoacoustic instability. To that end, using flow restrictors, we induce blockage in the inlet flow upstream of the swirler, perpendicular to the bulk flow direction. We observe that in one case, there is a reduction in the amplitude of the periodic oscillations while in the other case, there is a suppression of thermoacoustic instability. In the former case, the blockage in the inlet flow stream is more distributed, while in the latter, the same degree of blockage is clustered into one region of the inlet flow stream. The field of the local instantaneous acoustic energy production ($p'(t)q'(x, y, t)$) shows the presence of coherence during the occurrence of thermoacoustic instability for the experiments without any blockage. This emerging coherence is disrupted with the inclusion of the blockage. In the case with clustered blockage, the coherence is suppressed significantly, while for the case with the distributed blockage, it is reduced

^{*}Senior Scientist, Aerospace Engineering Department, IIT Madras

[†]Senior Scientist, Aerospace Engineering Department, IIT Madras

[‡]Project Scientist, Aerospace Engineering Department, IIT Madras

[§]Professor, Aerospace Engineering Department, IIT Madras, Associate fellow of AIAA

slightly. Analysis of spatial variance, performed on the local instantaneous acoustic energy production indicates the disruption of the coherent spatial structures with the flow restrictors, which subsequently suppresses thermoacoustic instability.

I. Introduction

Swirl-stabilized flames are often used in turbulent combustors due to its strong stabilizing effect on the flame.¹ However, when such combustors are operated at fuel lean conditions, they are prone to thermoacoustic instability.² This phenomenon arises due to the positive interaction between the unsteady heat release rate and the acoustic field of the combustion chamber.² Thermoacoustic instability occurs when the heat release rate fluctuations and the unsteady pressure fluctuations are in phase with each other.

Suppressing or controlling these large amplitude pressure oscillations is critical for the operation of the gas turbine engines as they cause structural failure to their components and unwanted shutdowns.³ There have been a number of studies which have investigated strategies to suppress thermoacoustic instability or to reduce the amplitude of the periodic oscillations.⁴⁻⁷ However, thermoacoustic instability is still difficult to predict and control due to its sensitivity to small changes in the system.⁸ Furthermore, the challenges faced in adapting control measures to commercial systems also make the elimination of thermoacoustic instability a difficult task. Effective methods to control or prevent thermoacoustic instability requires an exhaustive investigation of the transition from stable operation to unstable operation of the turbulent combustor.

Recently, it was observed that thermoacoustic systems undergo a transition from stochastic fluctuations near blowout conditions to periodic oscillations via low-dimensional chaotic oscillations as the equivalence ratio is increased.⁹ In another study on a turbulent combustor, it was observed that thermoacoustic instability is presaged by intermittency,^{10,11} wherein bursts of large amplitude periodic oscillations appear in an apparently random manner, amidst low amplitude aperiodic fluctuations. Using a flame describing function, Ebi et al.¹² suggested that during the intermittent oscillations, there is transition from the low amplitude regime to the large amplitude regime and vice versa due to the continuously varying phase difference between the acoustic pressure fluctuations and the heat release rate fluctuations. Nair et al.¹³ suggested that combustion noise, the stable state from which the transition to thermoacoustic instability takes place, has chaotic characteristics. Tony et al.¹⁴ showed that the pressure fluctuations during combustion noise contain features of high dimensional chaos, contaminated with white and colored noise. Additionally, spatial analysis on the relative phase between the acoustic pressure fluctuations and the heat release rate fluctuations

obtained from CH^* chemiluminescence of the flame showed that during the occurrence of intermittency, regions of coherent behaviour emerge amidst incoherent regions.¹⁵

From the perspective of dynamical systems theory, previous studies have shown that thermoacoustic systems undergo transitions from a stable operation to limit cycle oscillations through bifurcations. For instance, Lieuwen,¹⁶ reported supercritical and subcritical Hopf bifurcations in an experimental study of a premixed gas turbine combustor, wherein, the transition characteristics varied as a result of the different inlet velocities used in the combustor. An experimental study on a Rijke tube, a prototypical thermoacoustic system, showed that the criticality of the bifurcations (sub-critical or supercritical) is dependent on the Strouhal number.¹⁷ They observed that the transition characteristics transformed from a supercritical Hopf bifurcation to a sub-critical Hopf bifurcation with increase in the air flow rate.

Zinn and Lieuwen¹⁸ reported that the perturbations of the order of the background noise levels are sufficient to trigger a thermoacoustic system. Recently, studies were performed on simple laminar thermoacoustic systems to understand the effect of turbulence on the transition to thermoacoustic instability.⁸ For example, Waugh and Juniper¹⁹ demonstrated that additive stochastic perturbations can cause triggering from low noise amplitudes to self-sustained oscillations in a Rijke tube. Similarly, in a ducted non-premixed flame operating in a bistable region, it was found that under the influence of small amplitude noise, the system underwent a transition from a stable state to an oscillatory state.²⁰ Furthermore, Waugh and co-workers²¹ showed that triggering depends on the strength and the color of noise. They had observed that pink noise added to the thermoacoustic system is most effective in triggering the system to instability, whereas, blue noise could prevent the phenomenon of triggering.

Studies have shown that for thermoacoustic systems undergoing a subcritical Hopf bifurcation, the hysteresis width decreases with increase in the noise intensities.^{22,23} Further, Gopalakrishnan and co-workers²² observed that once the intensity of noise is beyond a threshold value, the subcritical transition is not discernible and appears continuous. However, Waugh and co-workers^{19,21} observed that the amplitude of the limit cycle oscillations is not altered by the addition of noise. Jagadesan and Sujith²⁰ observed that increasing the noise intensity on a non-premixed ducted flame results in a drift of the phase difference between the acoustic pressure fluctuations and the heat release rate fluctuations. This drift in the phase difference led to the reduction of the amplitude of the pressure oscillations.

A link between coherent structures in the flow field and thermoacoustic instability has been observed in the recent years. Schadow et al.²⁴ established large scale coherent structures in the flow field as the drivers of thermoacoustic instability. In addition, McManus and Bowman²⁵ observed that in a laboratory-scale dump combustor, combustion instability

increases, while using vortex generator jets inducing streamwise vorticity. Coherent vortices are observed in swirl-stabilized combustors with a sudden expansion region. These coherent vortices form in the separating shear layer due to the inherent Kelvin-Helmholtz instability.²⁶ At certain conditions, large scale vortex mixing could result in a periodic heat release rate which could then couple with the acoustic modes of the combustor duct, causing thermoacoustic instability.²⁷

Various studies have shown the mitigation of thermoacoustic instability by altering the flow field, which, in turn, alters the dynamics of the coherent flow structures. Paschereit et al.²⁸ observed that the suppression of thermoacoustic instability can be achieved by suppressing the formation of these coherent structures in the flow field. They successfully devised an active control method to modulate the air flow and thereby vary the mixing process between the reactants and the combustion products which results in the reduction of the coherence of the vortical structures. Additionally, Schadow et al.²⁹ used triangular jets in a dump combustor to suppress the large amplitude pressure oscillations. Here, the injection of the fuel into the corners of the triangle instead of the flat sides resulted in a significant reduction of the amplitude of the pressure oscillations. Furthermore, Paschereit and Gutmark³⁰ developed a passive control method wherein large scale vortices formed by pairing and vortex merging were disrupted by the use of distributed vortex generators. These vortex generators interrupt the roll up of the vortices by the introduction of streamwise vorticity.

Essentially, in gas turbine engines, the large amplitude periodic oscillations occur due to a positive feedback between the acoustic pressure fluctuations and the heat release rate fluctuations, amidst a turbulent flow field. Various reduced order models and experimental studies on prototypical systems, with compact heat sources have exhibited many characteristics of a thermoacoustic system.^{31–34} However, a turbulent flame is not compact, but spatially extended, wherein it interacts with the local flow dynamics and the acoustic perturbations. These interactions occur at every point in space and in time. It is important to account for these spatiotemporal interactions for the design of control strategies to prevent the onset of thermoacoustic instability. We utilize flow restrictors with different configurations to modify the spatial flow dynamics. We find that the spatial dynamics of the flow field plays a significant role in controlling the transition to thermoacoustic instability.

Using the flow restrictors, we vary the configuration of the blockage in the flow stream upstream of the swirler. We find that on utilizing the flow restrictors with a clustered configuration of the blockage, there is a suppression of thermoacoustic instability, while with the distributed blockage, there is only a reduction of the amplitude of the limit cycle oscillations. In particular, we investigate the spatial dynamics in the field of the instantaneous local acoustic power production $p'(t)\dot{q}'(x, y, t)$ for the different cases to understand this transition.

We also examine the evolution of the spatial dynamics using spatial variance to identify the spatially coherent structures and characterize the transition.

Section 2 describes the experimental setup of the turbulent combustor with a swirl-stabilized flame and the data recording systems. Section 3 details the results and the analyses from the experiments. We draw the major conclusions from the study in Section 4.

II. Experimental Setup

We use the turbulent combustor shown in Fig. 1a with a fixed vane swirler for flame stabilization. The length of the swirler is 30 *mm*. It is located in the burner assembly which is illustrated in Fig. 1b. The swirler has 8 fixed vanes of 1 *mm* thickness. The vanes are bent to impart radial momentum to the incoming flow. The swirler is mounted on a central shaft. A center body which is 30 *mm* long and has a diameter of 16 *mm* is located downstream of the swirler for flame stabilization. The center body is mounted such that it is flushed with the exit plane of the burner. A flame arrestor is located upstream of the swirler to prevent flashback. The combustor duct has a cross section of 90×90 *mm*² and is 1100 *mm* long. A spark plug is mounted on the dump plane to ignite the fuel/air mixture. A decoupler is located at the end of the combustion chamber to replicate the boundary condition of an open duct ($p' = 0$) as well as to reduce the acoustic losses to the surroundings due to acoustic radiation.

Liquefied Petroleum Gas (LPG), partially premixed with air, is used as the combustible mixture for the experiments. The composition of LPG used is approximately 60% butane and 40% propane. Fuel is injected 100 *mm* upstream of the swirler while air enters through the plenum chamber. In this study, for all the experiments, the fuel flow rate is fixed and the air flow rate is varied. In this manner, the equivalence ratio is varied from the stoichiometric ratio to lean ratios. The equivalence ratio is calculated as $\phi = (\dot{m}_f/\dot{m}_a)_{\text{actual}} / (\dot{m}_f/\dot{m}_a)_{\text{stoichiometric}}$ where \dot{m}_f and \dot{m}_a are the mass flow rates of fuel and air respectively. These mass flow rates are controlled by mass flow controllers of Alicat Scientific MCR Series. The mass flow controllers have uncertainties of 0.8% of the reading + 0.2% of the full scale. Subsequently, the maximum uncertainty in the calculated equivalence ratio for all the flow rates is ± 0.03 . Here, we perform the experiments with the mass flow rate of fuel fixed at 4.96×10^{-4} kg/sec, which corresponds to a thermal power of 24.7 KW. The flow rates used in our study correspond to *Re* between 10000 and 20000 (uncertainty of 6% due to uncertainties in the mass flow rate measurements).

Unsteady pressure signals p' are measured using a piezoelectric transducer PCB103B02, which has an uncertainty of ± 0.15 *Pa*. The transducer is mounted 17 *mm* downstream of the dump plane. The mounting arrangement of the transducer results in an acoustic phase

delay of 5° , which is not large enough to affect the analyses of the current study. The signals from the pressure transducer are acquired using an A-D card (NI-6143 - 16 bit) at a sampling frequency of 10 kHz for three seconds.

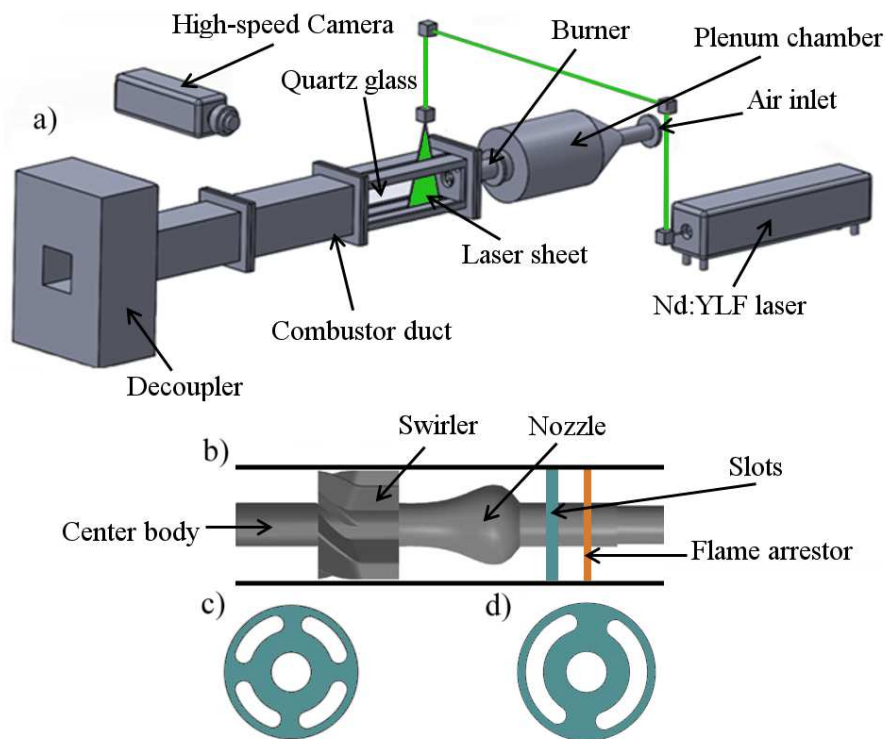


Figure 1. a) Schematic of the turbulent combustor, based on the original design of Komarek and Polifke.³⁵ Air enters through the plenum chamber while the fuel enters at the burner. An Nd:YLF Laser is used for the cold flow PIV experiments. A high-speed camera is used for capturing the Mie scattered images and the CH^* chemiluminescence. b) the schematic of the burner assembly where the flow direction is from the right to the left, c) the slot configuration corresponding to case II, d) the slot configuration corresponding to case III.

The flow restrictors used in our experiments to vary the blockage of the inlet flow stream and the resulting flow dynamics in the combustor duct is inspired from the works of Marshall et al.,³⁶ Videto and Santavicca³⁷ and Coppola and Gomez³⁸ on a turbulence generator for combustion systems. Using this turbulent flow system, the turbulence intensity can be varied without changing the mean flow velocity. The turbulence generator comprises of slots used to block the incoming flow, located upstream of a contoured nozzle as shown in Fig. 1b. The blockage can be varied by changing the angle between the slots. The principle behind the design is as follows. Vortices are produced at the slots due to the blockage of the flow. These vortices disintegrate into smaller vortices upon impingement, through a turbulent cascade process, producing fine scale turbulence. The turbulence intensity in the combustion chamber can be increased by increasing the blockage of the flow using the slots. In our experiments, we try to use these slots to vary the flow dynamics near the dump plane of the combustor. Initially, we perform experiments without the flow restrictors. This case

is referred to as case I. The blockage used for the experiments with the turbulence generator is approximately 75% of the burner cross section. The experiments with the configuration shown in Fig. 1c is referred to as case II while those with the configuration shown in Fig. 1d is referred to as case III. The configuration shown in Fig. 1c induces blockage in the horizontal and the vertical direction while that shown in Fig. 1d provides the same blockage, but only in the vertical direction.

Cold flow Particle Image Velocimetry (PIV) experiments are performed on the section of the combustor made of quartz. A single cavity-double pulsed laser (Photonics DM527-50) of an operating wavelength of 527 nm is used with a repetition rate of 4 kHz to produce the laser pulses needed for illuminating the seeding particles. This results in 2000 velocity fields per second. The time duration between the two laser pulses is maintained at 30 μ s to achieve the required displacement (maximum of 4 pixels) of the seeding particles. This low value of particle displacement, is used to reduce the velocity uncertainties due to the out of plane movement of the seeding particles.³⁹ Three right angle prisms and a pair of convex lenses of focal lengths 500 mm and 50 mm are used to direct the laser beam towards the combustor duct and to reduce the divergence of the laser beam respectively. Spherical and cylindrical lenses of focal lengths 600 mm and -16 mm are utilized to expand the laser beam into a laser sheet having a thickness of 2 mm. The laser sheet is then transmitted into the combustion chamber through a horizontal slit of 5 mm width and 400 mm length. Olive oil droplets, which are produced using a Laskin nozzle are used as the seeding particles and have a size of approximately 1 μ m. A high-speed CMOS camera (Phantom V 12.1), operated at 1280 \times 800 pixels, is used to capture the Mie scattered light onto single frame-single exposed images. The camera is outfitted with a ZEISS camera lens having of focal length of 50 mm with the aperture at f/5.6. As a result, a section of the combustor duct, having the dimensions of 126 mm \times 90 mm is imaged on the camera sensor. A bandpass optical filter centered at 527 nm (10 nm FWHM) is mounted on the camera lens to capture the light scattered from the oil particles. The seeding particle density was large enough to achieve more than the required particles in the interrogation windows for the PIV image processing.

The images obtained from the cold flow PIV experiments are processed using the PIVview software from PIVtech GmBh.⁴⁰ The images are divided into interrogation windows of 32 \times 32 pixels with 50% overlap in the x and y direction. Cross-correlation technique with a multi-pass approach (3 passes) is used for the statistical PIV evaluation.⁴¹ The least square Gaussian fit peak search scheme is used as the peak detection scheme.⁴¹ In total, less than 1% of the velocity vectors evaluated are detected as outliers and are replaced using a bilinear interpolation method. A subpixel accuracy of 0.1 pixel is possible with interrogation windows of 32 \times 32 pixels. Consequently, for the maximum particle displacement of 4 pixels, the velocity uncertainty is calculated to be 2.5%. The particle sizes on the recorded images

are approximately between 2 and 3 pixels. This results in an uncertainty of 0.1 pixels due to peak locking effects.⁴² If we consider a maximum out-of-plane movement of 4 pixels, we expect an uncertainty of 0.2 pixels for particle image sizes of 2.5 pixels.⁴² This results in an uncertainty of 5%. Further, low velocity regions in the flow field have a pixel displacement of 0.2 pixels which could result in large uncertainties of 50%.

For the hot flow experiments, a high-speed CMOS camera (Phantom v 12.1) is used to acquire the flame images. It is operated at 1280×400 pixels. A narrow band pass filter centered at 435 nm (10 FWHM) is used to capture the CH^* chemiluminescence intensities. The camera is operated at a sampling rate of 2 kHz. It is outfitted with a ZEISS 50 mm camera lens with the aperture at f/2. Subsequently, a section of the combustor, $280 \text{ mm} \times 90 \text{ mm}$ is imaged on 870×280 pixels of the camera sensor.

III. Results

Essentially, this experimental study investigates the effect of the turbulent flow field on the global dynamics of a turbulent combustor. To that end, we investigate three cases in this experimental study. The first case, referred to here as case I refers to experiments performed without the turbulence generator assembly and hence, without any blockage in the flow stream. Correspondingly, the burner contains only the swirler, the flame arrestor and the center body. Case II and case III correspond to the experiments performed with the turbulence generator. The blockage ratio using the slots is the same for these two cases. However, the blockage is induced differently for cases II and III. For case II, the slots are arranged in such a way that there is blockage in the horizontal and as well as the vertical direction, while in case III, the slots are arranged next to each other such that the blockage is only in the vertical direction. The configuration for case II is such that the blockage is distributed in the azimuthal direction. However, for case III, there is a large blockage in one region of the inlet flow. These configurations result in different spatial flow dynamics in the combustor duct.

Cold flow experiments (without the flame) are conducted to acquire PIV data and analyse the flow dynamics in the combustion chamber without the presence of thermoacoustic feedback. The time-averaged turbulence intensity fields and the corresponding time-averaged vorticity fields for each case are depicted in Fig. 2. The flow rates used for these cold flow experiments are fixed corresponding to the air flow rates used at the equivalence ratio $\phi = 0.46$. The bulk flow of the fluid stream is from left to right and the dump plane aligns with the the vertical plane at $x = 0$. The time-averaged turbulence intensity at each location in the image is obtained by calculating the ratio between the velocity fluctuations u' and v' (rms) at that location, and the bulk flow velocity at the burner exit. Turbulence intensity

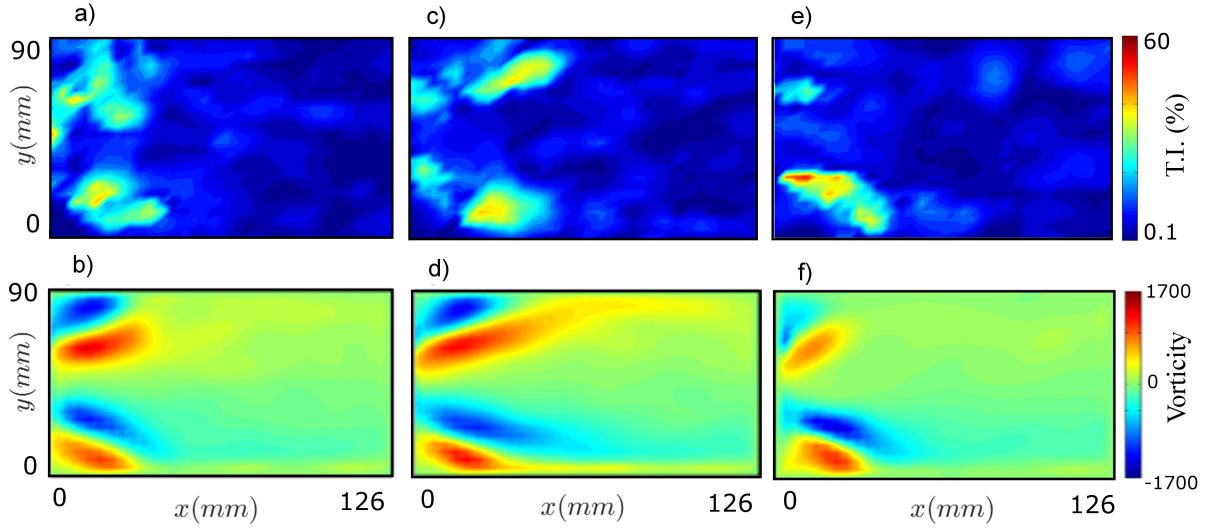


Figure 2. Time-averaged turbulence intensity fields - T.I. (a, c, e) and the corresponding time-averaged vorticity fields (b, d, f) obtained from the cold flow experiments. (a, b) correspond to case I, (c, d) refer to case II and (e, f) correspond to case III. x refers to the distance from the dump plane while y refers to the distance in the vertical direction.

(T.I) is defined as $T.I = \sqrt{(u'/U)^2 + (v'/U)^2}$. Figures 2(a, b) correspond to case I. Figures 2(c, d) refer to case II while figures 2(e, f) refer to case III. Compared to case I, case II depicts higher turbulence intensity and vorticity strength downstream of the dump plane. Further, it appears that the higher turbulence intensities are located further downstream in comparison to the field for case I. In case III, there appears to be higher turbulence intensity below the horizontal axis compared to that above. This could be the result of imaging performed in a non-symmetric manner. Thus, the different configurations using the slots results in different distributions of the turbulence intensity in the combustor duct.

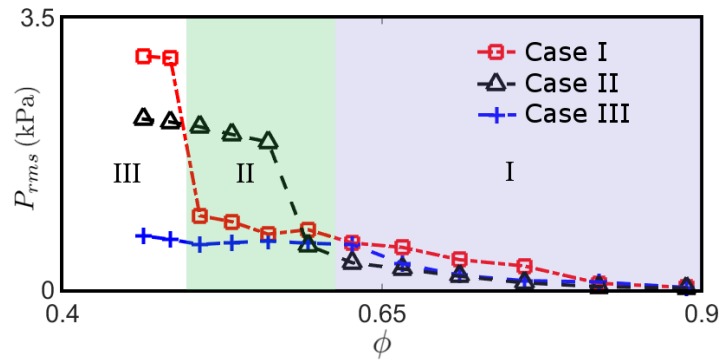


Figure 3. Variation of the root mean square of the unsteady pressure fluctuations, P_{rms} , as a function of the equivalence ratio ϕ for case I ($-\square-$), case II ($-\triangle-$) and case III ($-+-$).

Figure 3 depicts the variation of the root mean square (P_{rms}) of the unsteady pressure fluctuations p' as a function of the equivalence ratio ϕ for the three cases. We observe three zones corresponding to different ranges of equivalence ratios. As the equivalence ratio is reduced for case I, there is a gradual increase in the P_{rms} observed in zones I and II. At zone

III, there is a sudden increase in the value of the P_{rms} for case I. Considering the plot for case II, the value of P_{rms} is lower than that of case I in zone I. As the equivalence ratio is reduced, there is an increase in the P_{rms} in zone II, depicting an advanced onset of thermoacoustic instability for case II. However, as the equivalence ratio is reduced further, the P_{rms} does not rise above that of case I in zone III. This behavior, observed in case II appears to be similar to that observed in the studies on the effect of noise on the transitions in thermoacoustic systems where they have observed an advanced onset of thermoacoustic instability and a reduction in the strength of the pressure oscillations (P_{rms}), with the addition of noise.^{20,22}

Examining the results for case III, we find that the value of the P_{rms} is less than that of case I in zone I while it is similar to that of case II till $\phi = 0.65$. As ϕ is reduced, the value of P_{rms} is significantly lower than that of case II while it is slightly lower than that of case I. With a further reduction in ϕ , the P_{rms} remains low. The P_{rms} corresponding to case III at this low equivalence ratio is approximately 77% lower than that of case I and 68% lower than that of case II. Thus, the introduction of the blockage, using the turbulence generator, results in new dynamics at low equivalence ratios wherein the self-sustained large amplitude periodic oscillations are suppressed for case III and strength of the oscillations are reduced for case II. We have repeated these experiments and we observe similar trends in the strength of the pressure oscillations.

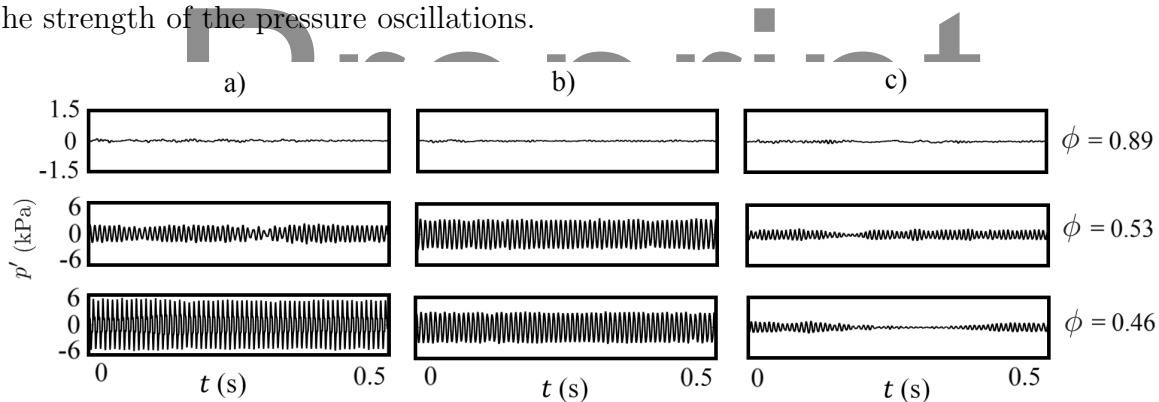


Figure 4. Unsteady pressure fluctuations for varying equivalence ratios for case I (a), case II (b) and case III (c).

The unsteady pressure fluctuations acquired using the piezoelectric transducer for the different cases at varying equivalence ratios are presented in Fig. 4. At $\phi = 0.89$, we observe low amplitude aperiodic fluctuations corresponding to the state of combustion noise for all three cases. At $\phi = 0.53$, periodic oscillations are observed for case II while there appears to be short epochs of aperiodic dynamics for case I. Nevertheless, the amplitude of the pressure oscillations is higher for case II, which is in accordance with the advanced onset of thermoacoustic instability as observed from Fig. 3. In addition, the unsteady pressure signals for case III at $\phi = 0.53$ appear intermittent and moreover, the amplitude of the pressure oscillations is lower. As the equivalence ratio is reduced further to $\phi = 0.46$, maximum

amplitude of the pressure oscillations is observed to be higher for case I when compared to those of case II and case III. Further, the pressure oscillations remain intermittent for case III and more importantly, the amplitude of the oscillations is significantly lower than that of the other two cases. Thus, case II results in an advanced onset of self-sustained periodic oscillations but with a reduced amplitude of pressure oscillations. However, case III results in the suppression of thermoacoustic instability and the pressure oscillations remain intermittent even at low equivalence ratios. These results highlight the need to investigate the spatial dynamics to understand the reasons for the advanced onset of thermoacoustic instability in case II and suppression of the limit cycle oscillations in case III. A measure, which provides a preliminary understanding of these spatial interactions is $p'(t)q'(x, y, t)$. This term is the instantaneous local acoustic driving, which is equivalent to the Rayleigh criterion when integrated over time and space.

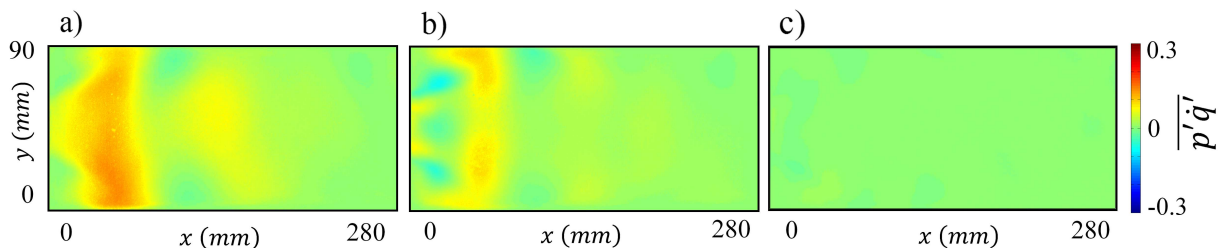


Figure 5. Time-averaged $\overline{p'q'}$ for case I (a), case II (b) and case III (c) at $\phi = 0.46$.

The time-averaged local acoustic power production ($\overline{p'q'}$) is shown for the different cases at $\phi = 0.46$ in Fig. 5. It is calculated by using the product of the acoustic pressure fluctuations $p'(t)$ and the local heat release rate fluctuations $q'(x, y, t)$, which is subsequently averaged over time. One can observe regions of similar positive values near the dump plane for case I in Fig. 5a. These regions have positive values and hence drive the acoustic pressure oscillations at thermoacoustic instability. Further, the spatial distribution of $\overline{p'q'}$ shows the presence of the axial mode of instability. One could conjecture that the coherent flow structures which form in the combustor duct are responsible for the emergence of large regions with positive values. These coherent flow structures bring in fresh reactants and mix with the hot radicals in the recirculation zones. On the impingement of these flow structures on the combustor walls, or the breakdown of these flow structures, simultaneous reaction could occur, leading to large positive regions in the field of $\overline{p'q'}$, provided that the pressure oscillations and the local heat release rate oscillations are in phase. Further, these regions seem to be repeating downstream in the combustor duct for case I. However, in case II, these regions with positive values of $\overline{p'q'}$ appear to be smaller in size and in strength as depicted in Fig 5b. Further, it appears that there are regions of negative acoustic driving near the dump plane for case II. The decrease in the size and strength of these positive

regions corresponds to the reduction in the P_{rms} observed for case II at $\phi = 0.46$.

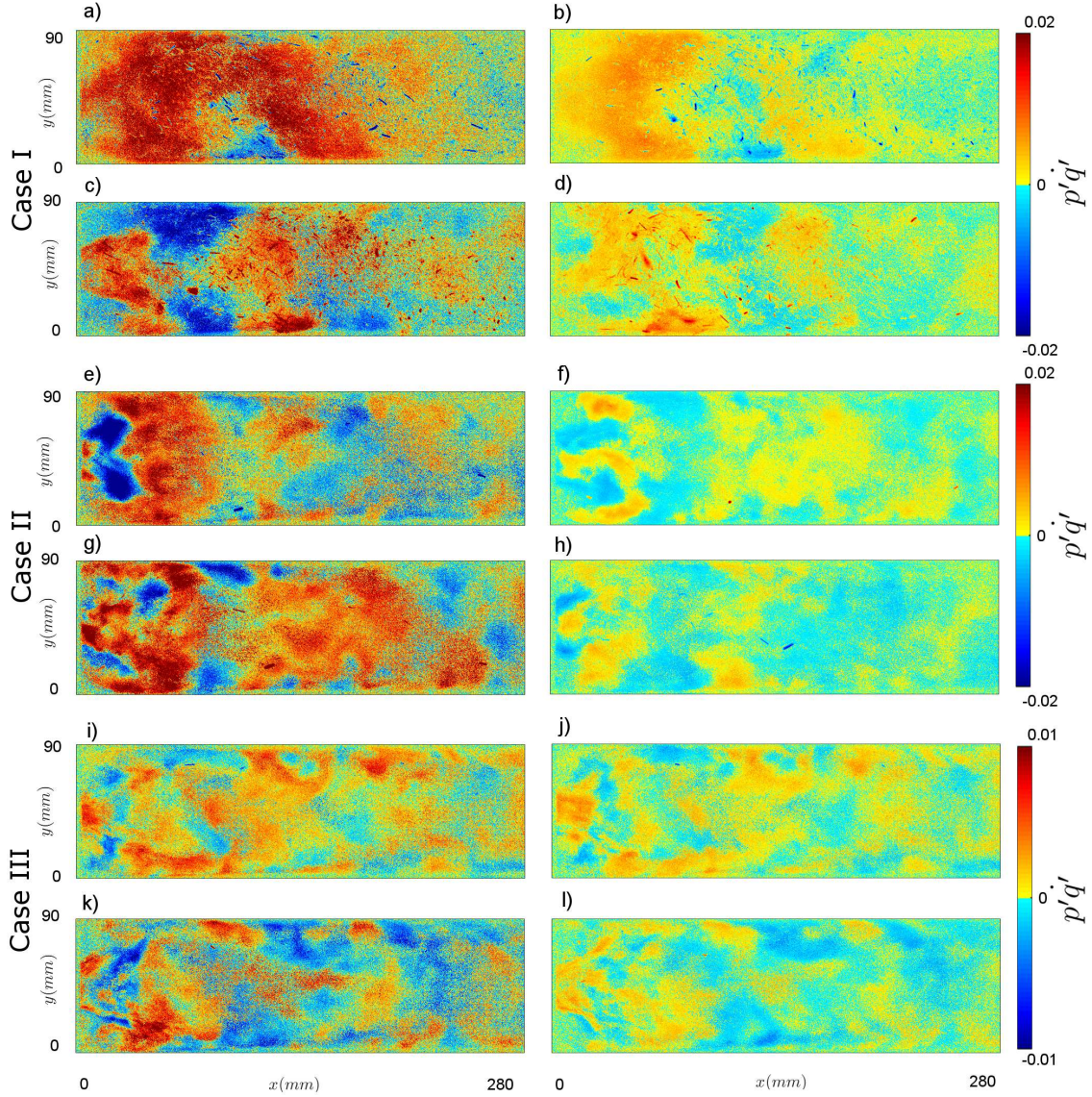


Figure 6. Instantaneous $p'(t)\dot{q}'(x, y, t)$ (a-d) case I, (e-h) case II and (i-l) case III at $\phi = 0.46$. a-d and e-h correspond to one periodic cycle of oscillation during thermoacoustic instability for cases I and II. i-l correspond to a periodic cycle during the periodic epoch of the intermittent dynamics for case III.

Furthermore, in Fig 5c, the local acoustic power production for case III appears to have low strength. Further, the large regions of high positive values are not observed anymore. Thus, the blockage configuration in case III results in the suppression of thermoacoustic instability at low equivalence ratios. A numerical study was performed by Eisenhower et al.,⁴³ where they modeled the thermoacoustic dynamics of an annular combustor using a coupled oscillator system which includes a parameter for the spatial symmetry of the passive dynamics. They observed that the spatial perturbation of the symmetry of the acoustic wavespeed reduces the amplitude of the limit cycle. In essence, this study showed the importance of the spatial dynamics on the suppression of thermoacoustic instability. In the

field of $\overline{p'q'}(x, y)$, the positive regions of $p'q'$ reflect the presence of local acoustic driving (pressure fluctuations and local heat release rate fluctuations are in phase with each other locally). These interactions are constructive because they result in the transfer of energy to the acoustic field, which would subsequently perturb the flame appropriately and complete the positive feedback loop. Further, these local interactions between the flame, the acoustic field and the flow dynamics result in the emergence of the large regions of positive values. However, one could argue that the suppression of thermoacoustic instability in case III is possibly due to the reduction in the constructive interactions causing a suppression of the periodic formation of the coherent flow structures in the combustor duct.^{24,28} Subsequently, the suppression of the coherent flow structures changes the distribution of the local heat release rate leading to the disruption of the regions of positive $p'q'$ in the local acoustic power production.

The instantaneous plots of $p'(t)q'(x, y, t)$ are illustrated in Fig. 6 for $\phi = 0.46$ for the three cases. We observe large regions of similar values of positive $p'q'$ for case I at certain instants. Further, it appears that the field at a), contains a large region of similar positive values of $p'q'$ near the dump plane. The similarity in the values reflects the spatial coherence of $p'q'$. However, further downstream, we observe grainy regions. Similarly, we observe regions of coherence of positive values for case II. However, the regions appear to be smaller and more dispersed than case I. These regions of coherence extend downstream of the duct. Further, we observe strong negative values of $p'q'$ near the dump plane for case II. The $p'(t)q'(x, y, t)$ fields for case III show highly dispersed positive regions and is dominated by grainy regions near the dump plane. Further, the magnitude of the positive regions are lower compared to the other cases. These instantaneous plots signify the importance of the emergence of these coherent regions for the occurrence of large amplitude periodic oscillations.

The spatial plots of the time-averaged local acoustic power production illustrate the formation of the coherent spatial structures and its strength is synonymous with thermoacoustic instability. To improve our understanding of the spatial dynamics, we perform spatial analysis on the instantaneous local acoustic power production. Spatial statistics such as spatial variance, spatial correlation and spatial skewness are calculated and adopted in studying transitions in many complex ecological systems.⁴⁴ In our study, we investigate the spatial dynamics using spatial variance of the instantaneous local acoustic power production. Spatial variance have been used in the past to study the formation of coherent regions in systems undergoing transitions to new dynamical states. Hence, we use spatial variance to investigate the formation of coherent spatial structures in the field of $p'q'(x, y, t)$. Spatial variance of $p'(t)q'(x, y, t)$ is calculated as $\sigma(t) = \frac{1}{N} \sum_x \sum_y (p'(t)q'_{xy}(t) - \langle p'(t)q'(t) \rangle)^2$ where $p'(t)q'_{xy}(t)$ is the instantaneous local acoustic power production, $\langle p'(t)q'(t) \rangle$ is the instantaneous spatially averaged acoustic power production and N is the total number of pixels.

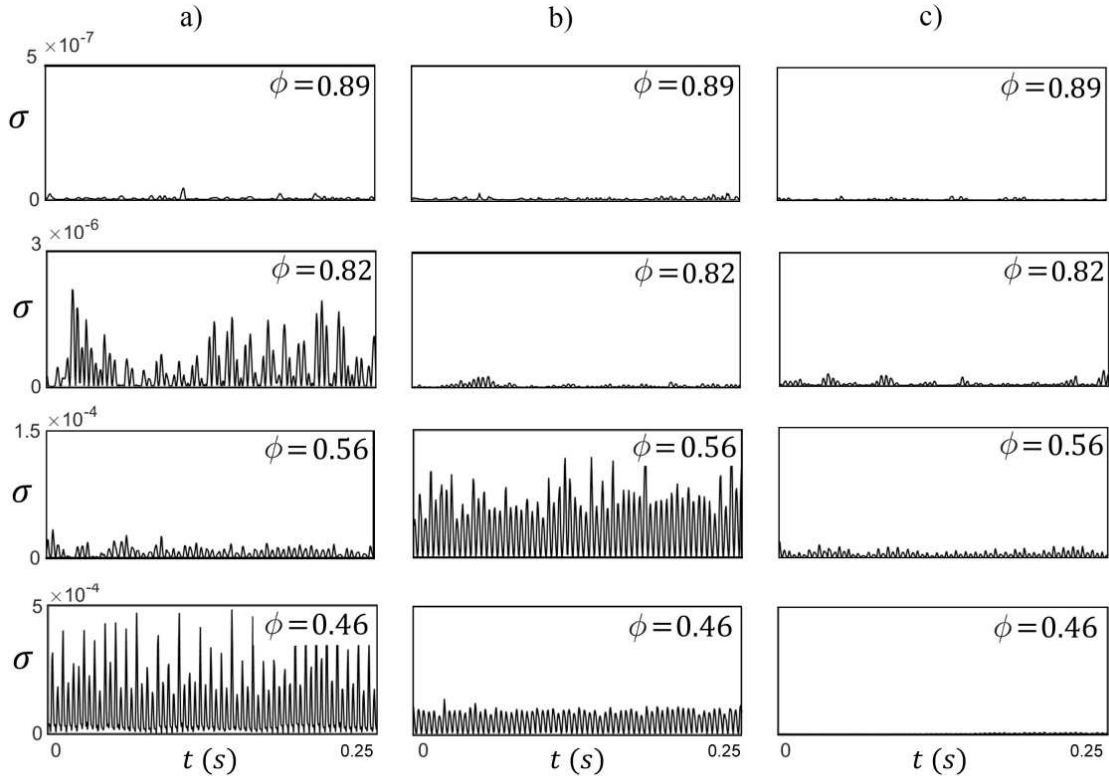


Figure 7. Spatial variance a) case I, b) case II and c) case III for different ϕ . Note that the abscissa is different for the different ϕ .

The spatial variance $\sigma(t)$ is plotted for various equivalence ratios in Fig. 7 for case I (a), case II (b) and case III (c). We observe that, in general, the spatial variance $\sigma(t)$ increases with decrease in the equivalence ratio for case I and case II. Further, the spatial variance appears to alternate between high and low values. The time series of the spatial variance of $p'(t)\dot{q}'(x, y, t)$ at $\phi = 0.46$ for case I illustrates the effect of the impingement of the large scale vortices, causing simultaneous reaction, resulting in momentary coherence of $p'(t)\dot{q}'(x, y, t)$ during the occurrence of thermoacoustic instability (for one periodic cycle). At $\phi = 0.56$, the spatial variance is larger for case II when compared to case I. This indicates that the onset of the formation of coherent spatial structures is advanced, that is, coherence emerges at higher ϕ for case II when compared to case I. However, one can observe that for case III, the spatial variance is significantly lower in magnitude than the other two cases especially at lower equivalence ratios. This shows that the coherent spatial structures are suppressed in the field of $p'\dot{q}'(x, y, t)$ for case III.

IV. Conclusion

In this experimental study, we investigate the effect of the distribution of the turbulence intensity on the transition from combustion noise to thermoacoustic instability in a swirl-

stabilized combustor. Three different cases are studied. The first case, referred to as case I, exhibits the transition from combustion noise to thermoacoustic instability. A turbulence generator is used in the cases II and III to vary the flow dynamics in the combustor duct. We compare the results obtained for case I with cases II and III. Using the turbulence generator, we induce a blockage in the flow in the vertical and horizontal direction for case II while the same blockage is induced only in the vertical direction for case III. In this manner, for case II, the blockage is distributed, while for case III, there is a large blockage in one region of the inlet flow. We perform PIV experiments to characterize the turbulence levels for different configurations of the turbulence generator. We acquire unsteady pressure signals and high-speed CH^* chemiluminescence images which are representative of the local heat release rate for the combustion experiments.

We observe that in case II, there is an advanced onset of large amplitude periodic oscillations. However, we observe that the amplitude of oscillations is lower when compared to the case without any blockage at lower equivalence ratios (case I). Further, we observe that the turbulence generator configuration for case III results in the suppression of thermoacoustic instability. Here, the acoustic pressure oscillations remain intermittent and the amplitude of these oscillations are significantly lower than the other two cases. The instantaneous plots of $p'(t)\dot{q}'(x, y, t)$ illustrate the formation of coherent regions near the dump plane for case I, while the coherence is dispersed for case II. Further, for case III the field of $p'(t)\dot{q}'(x, y, t)$ appears very grainy with only small regions of coherence throughout the duct. Additionally, using spatial variance of the field of $p'(t)\dot{q}'(x, y, t)$ which represents the local instantaneous acoustic power production, we find that coherent spatial structures form during the transition from combustion noise to thermoacoustic instability. We observe that the advanced onset of thermoacoustic instability for case II matches with the increase in the spatial variance. Additionally, when thermoacoustic instability is suppressed for case III, we observe that the spatial variance is low compared to the other two cases, depicting the suppression of coherent spatial structures.

Acknowledgments

The authors would like to acknowledge the European Commission under call FP7-PEOPLE-ITN-2012 within the Marie Curie Initial Training Network Thermo-acoustic and aero-acoustic nonlinearities in green combustors with orifice structures (TANGO) and the Gas Turbine Technology Enabling Initiative (GATET), India for financially supporting the study. We would also like to acknowledge Komarek and Polifke (TU Munich) for the combustor design. We thank Tim Lieuwen (Georgia Institute of Technology) for introducing us to the design of the turbulence generator. We wish to acknowledge Thilagaraj S for assisting in the

experiments and providing the drawing of the experimental setup.

References

- ¹Driscoll, J. and Temme, J., “Role of swirl in flame stabilization,” *49th AIAA Aerospace Sciences Meeting including the New Horizons Forum and Aerospace Exposition*, 2011, pp. 108.
- ²Sujith, R. I., Juniper, M. P., and Schmid, P. J., “Non-normality and nonlinearity in thermoacoustic instabilities,” *International Journal of Spray and Combustion Dynamics*, Vol. 8, No. 2, 2016, pp. 119–146.
- ³Candel, S., “Combustion dynamics and control: Progress and challenges,” *Proceedings of the combustion institute*, Vol. 29, No. 1, 2002, pp. 1–28.
- ⁴McManus, K. R., Poinso, T., and Candel, S. M., “A review of active control of combustion instabilities,” *Progress in Energy and Combustion Science*, Vol. 19, No. 1, 1993, pp. 1–29.
- ⁵Lang, W., Poinso, T., and Candel, S. M., “Active control of combustion instability,” *Combustion and Flame*, Vol. 70, No. 3, 1987, pp. 281–289.
- ⁶Noiray, N., Durox, D., Schuller, T., and Candel, S. M., “Dynamic phase converter for passive control of combustion instabilities,” *Proceedings of the Combustion Institute*, Vol. 32, No. 2, 2009, pp. 3163–3170.
- ⁷Richards, G. A., Straub, D. L., and Robey, E. H., “Passive control of combustion dynamics in stationary gas turbines,” *Journal of Propulsion and Power*, Vol. 19, No. 5, 2003, pp. 795–810.
- ⁸Juniper, M. P. and Sujith, R. I., “Sensitivity and Nonlinearity of Thermoacoustic Oscillations,” *Annual Review of Fluid Mechanics*, Vol. 50, No. 1, 2017.
- ⁹Gotoda, H., Nikimoto, H., Miyano, T., and Tachibana, S., “Dynamic properties of combustion instability in a lean premixed gas-turbine combustor,” *Chaos: An Interdisciplinary Journal of Nonlinear Science*, Vol. 21, No. 1, 2011, pp. 013124.
- ¹⁰Nair, V., Thampi, G., and Sujith, R. I., “Intermittency route to thermoacoustic instability in turbulent combustors,” *Journal of Fluid Mechanics*, Vol. 756, 2014, pp. 470–487.
- ¹¹Nair, V. and Sujith, R. I., “Identifying homoclinic orbits in the dynamics of intermittent signals through recurrence quantification,” *Chaos: An Interdisciplinary Journal of Nonlinear Science*, Vol. 23, No. 3, 2013, pp. 033136.
- ¹²Ebi, D., Denisov, A., Bonciolini, G., Boujo, E., and Noiray, N., “Flame Dynamics Intermittency in the Bi-Stable Region Near a Subcritical Hopf Bifurcation,” *ASME Turbo Expo 2017: Turbomachinery Technical Conference and Exposition*, American Society of Mechanical Engineers, 2017, pp. V04BT04A058–V04BT04A058.
- ¹³Nair, V., Thampi, G., Karuppusamy, S., Gopalan, S., and Sujith, R. I., “Loss of chaos in combustion noise as a precursor of impending combustion instability,” *International Journal of Spray and Combustion Dynamics*, Vol. 5, No. 4, 2013, pp. 273–290.
- ¹⁴Tony, J., Gopalakrishnan, E. A., Sreelekha, E., and Sujith, R. I., “Detecting deterministic nature of pressure measurements from a turbulent combustor,” *Physical Review E*, Vol. 92, No. 6, 2015, pp. 062902.
- ¹⁵Mondal, S., Unni, V. R., and Sujith, R. I., “Onset of thermoacoustic instability in turbulent combustors: an emergence of synchronized periodicity through formation of chimera-like states,” *Journal of Fluid Mechanics*, Vol. 811, 2017, pp. 659–681.
- ¹⁶Lieuwen, T. C., “Experimental investigation of limit-cycle oscillations in an unstable gas turbine combustor,” *Journal of Propulsion and Power*, Vol. 18, No. 1, 2002, pp. 61–67.

¹⁷Etikyala, S. and Sujith, R. I., “Change of criticality in a prototypical thermoacoustic system,” *Chaos: An Interdisciplinary Journal of Nonlinear Science*, Vol. 27, No. 2, 2017, pp. 023106.

¹⁸Zinn, B. T. and Lieuwen, T. C., “Combustion instabilities: Basic concepts,” *Combustion Instabilities in Gas Turbine Engines: Operational Experience, Fundamental Mechanisms, and Modeling*, Vol. 210, 2005, pp. 3–26.

¹⁹Waugh, I. C. and Juniper, M. P., “Triggering in a thermoacoustic system with stochastic noise,” *International Journal of Spray and Combustion Dynamics*, Vol. 3, No. 3, 2011, pp. 225–241.

²⁰Jegadeesan, V. and Sujith, R. I., “Experimental investigation of noise induced triggering in thermoacoustic systems,” *Proceedings of the Combustion Institute*, Vol. 34, No. 2, 2013, pp. 3175–3183.

²¹Waugh, I., Geuß, M., and Juniper, M., “Triggering, bypass transition and the effect of noise on a linearly stable thermoacoustic system,” *Proceedings of the Combustion Institute*, Vol. 33, No. 2, 2011, pp. 2945–2952.

²²Gopalakrishnan, E. A. and Sujith, R. I., “Effect of external noise on the hysteresis characteristics of a thermoacoustic system,” *Journal of Fluid Mechanics*, Vol. 776, 2015, pp. 334–353.

²³Moeck, J., Bothien, M., Schimek, S., Lacarelle, A., and Paschereit, C., “Subcritical thermoacoustic instabilities in a premixed combustor,” *14th AIAA/CEAS Aeroacoustics Conference (29th AIAA Aeroacoustics Conference)*, 2008, p. 2946.

²⁴Schadow, K. C. and Gutmark, E. J., “Combustion instability related to vortex shedding in dump combustors and their passive control,” *Progress in Energy and Combustion Science*, Vol. 18, No. 2, 1992, pp. 117–132.

²⁵McManus, K. R. and Bowman, C. T., “Effects of controlling vortex dynamics on the performance of a dump combustor,” *Symposium (International) on Combustion*, Vol. 23, Elsevier, 1991, pp. 1093–1099.

²⁶Coats, C. M., “Coherent structures in combustion,” *Progress in Energy and Combustion Science*, Vol. 22, No. 5, 1996, pp. 427–509.

²⁷Gutmark, E. J. and Grinstein, F. F., “Flow control with noncircular jets 1,” *Annual review of fluid mechanics*, Vol. 31, No. 1, 1999, pp. 239–272.

²⁸Paschereit, C. O., Gutmark, E., and Weisenstein, W., “Coherent structures in swirling flows and their role in acoustic combustion control,” *Physics of Fluids*, Vol. 11, No. 9, 1999, pp. 2667–2678.

²⁹Schadow, K. C., Gutmark, E. J., Wilson, K. J., and Smith, R. A., “Noncircular inlet duct cross-section to reduce combustion instabilities,” *Combustion Science and Technology*, Vol. 73, No. 4-6, 1990, pp. 537–553.

³⁰Paschereit, C. O. and Gutmark, E. J., “Control of high-frequency thermoacoustic pulsations by distributed vortex generators,” *AIAA journal*, Vol. 44, No. 3, 2006, pp. 550–557.

³¹King, L. V., “On the convection of heat from small cylinders in a stream of fluid: determination of the convection constants of small platinum wires with applications to hot-wire anemometry,” *Philosophical Transactions of the Royal Society of London. series A, containing papers of a mathematical or physical character*, Vol. 214, 1914, pp. 373–432.

³²Heckl, M. A., “Non-linear acoustic effects in the Rijke tube,” *Acta Acustica united with Acustica*, Vol. 72, No. 1, 1990, pp. 63–71.

³³Matveev, K. I., *Thermoacoustic instabilities in the Rijke tube: experiments and modeling*, Ph.D. thesis, California Institute of Technology, 2003.

³⁴Seshadri, A., Nair, V., and Sujith, R. I., “A reduced-order deterministic model describing an intermittency route to combustion instability,” *Combustion Theory and Modelling*, Vol. 20, No. 3, 2016, pp. 441–456.

³⁵Komarek, T. and Polifke, W., “Impact of swirl fluctuations on the flame response of a perfectly pre-mixed swirl burner,” *Journal of Engineering for Gas Turbines and Power*, Vol. 132, No. 6, 2010, pp. 061503.

³⁶Marshall, A., Venkateswaran, P., Noble, D., Seitzman, J., and Lieuwen, T. C., “Development and characterization of a variable turbulence generation system,” *Experiments in Fluids*, Vol. 51, No. 3, 2011, pp. 611–620.

³⁷Videto, B. D. and Santavicca, D. A., “A turbulent flow system for studying turbulent combustion processes,” *Combustion Science and Technology*, Vol. 76, No. 1-3, 1991, pp. 159–164.

³⁸Coppola, G. and Gomez, A., “Experimental investigation on a turbulence generation system with high-blockage plates,” *Experimental Thermal and Fluid Science*, Vol. 33, No. 7, 2009, pp. 1037–1048.

³⁹Pruvost, J., Legrand, J., Legentilhomme, P., and Doubriez, L., “Particle image velocimetry investigation of the flow-field of a 3D turbulent annular swirling decaying flow induced by means of a tangential inlet,” *Experiments in fluids*, Vol. 29, No. 3, 2000, pp. 291–301.

⁴⁰PIVview, *PIVTEC GmbH*, Homepage: <http://www.pivtec.com>, 2014.

⁴¹Raffel, M., Willert, C. E., Kompenhans, J., et al., *Particle Image Velocimetry: A Practical Guide*, Springer Science & Business Media, 2007.

⁴²Wieneke, B., “Generic a posteriori uncertainty quantification for PIV vector fields by correlation statistics,” *17th International Symposium on Applications of Laser Techniques to Fluid Mechanics (Lisbon, Portugal)*, 2014.

⁴³Eisenhower, B., Hagen, G., Banaszuk, A., and Mezić, I., “Passive control of limit cycle oscillations in a thermoacoustic system using asymmetry,” Tech. rep., DTIC Document, 2006.

⁴⁴Kéfi, S., Guttal, V., Brock, W. A., Carpenter, S. R., Ellison, A. M., Livina, V. N., Seekell, D. A., Scheffer, M., van Nes, E. H., and Dakos, V., “Early warning signals of ecological transitions: methods for spatial patterns,” *PloS one*, Vol. 9, No. 3, 2014, pp. e92097.